Hindawi
Geofluids
Volume 2022, Article ID 5178989, 10 pages
https://doi.org/10.1155/2022/5178989

Research Article

Description and Dynamic Analyses of the 1935 Luchedu Rock Avalanche in Sichuan, China

Jie Cui,[1] Chunyu Gao,[2,3] Zhilong Zhang,[2,3] and Guifu Xiang[1]

[1]*School of Southwest Univ. of Sci. and Technol, Mianyang 621010, China*
[2]*College of Water Resource & Hydropower, Sichuan Univ, Chengdu 610065, China*
[3]*State Key Lab. of Hydraulics and Mountain River Eng., Sichuan Univ, Chengdu 610065, China*

Correspondence should be addressed to Chunyu Gao; chygao@scu.edu.cn

Received 24 February 2022; Accepted 26 May 2022; Published 7 July 2022

Academic Editor: Peng Hou

Copyright © 2022 Jie Cui et al. This is an open access article distributed under the Creative Commons Attribution License, which permits unrestricted use, distribution, and reproduction in any medium, provided the original work is properly cited.

The Luchedu rock avalanche (LRA) that occurred in 1935 at the junction of Sichuan and Yunnan in Southwest China is a disaster chain of the rock slide, debris avalanche, and river blocking induced by heavy rainfall. The rock slide originated from the wedge formed by sheet metamorphic rocks on the fault zone on the left bank of the Jinsha River. After breaking away from the slope, the wedge disintegrated and cracked rapidly, forming debris and causing them to flow in fluidization along a 7.3 km path. After the obvious entrainment process and curve superelevation in the proximal area, the deposition reached 50.5×10^6 m^3 in the distal area. The sedimentary structure of clasts has typical stratification characteristics. The types of sedimentary facies include carapace facies, body facies, and mixed facies. Inside the sedimentary structure, dense shear zones, liquefied intercalations, jigsaw structures, and directional arrangement of particles are observed. Through a detailed geological survey and DEM spatial analysis, the avalanche entrainment rate of LRA was determined as 1.2. The morphological fluctuation of basement lithology and gully path plays an important role in the long-distance movement. The rock fragments formed by metamorphic rocks with a primary schistosity structure can effectively reduce the energy loss in the internal shear process and significantly promote the laminar flow movement in the distal region of the avalanche. Therefore, as a giant rock avalanche formed by the evolution of specific metamorphic rocks, LRA results from the combination of macrohydrodynamics and microrock failure properties.

1. Introduction

According to historical records, on December 22, 1935, a large-scale slope disaster broke out on the right bank of Jinsha River upstream of the Baini Cave in Xintian village, Huidong County, Sichuan Province. A large amount of debris was washed down at high speed along the 7.3 km Valley, destroying Upper Yanba village and Lower Yanba village on the right bank, reaching the opposite bank of Jinsha River to form a dam blocking the river. Three days later, the dam collapsed and caused 280 deaths. The disaster was called Luchedu landslide afterwards, named after the ferry located in the Jinsha River at Goukou. Luchedu landslide is on the eastern edge of the Qinghai Tibet Plateau. A few similar severe slope disasters occurred there, including the Lannigou landslide and Yigong landslide [1–4], all of which evolved from rock slides or rock falls at the beginning to a disaster chain event of dam building, river blocking, and collapse. Through field investigation, the Luchdu landslide had the characteristics of high speed and fluidization and was full of detritus, feasible to be categorized as a rock avalanches or debris avalanches.

Debris avalanches, rapid debris flow, and rock avalanches formed after the stability loss of some mines and loose filler slopes are some of the most dangerous and destructive phenomena of slopes in the world. As reported in the literature, rock avalanches or debris avalanches are extremely rapid, massive, flow-like motions of fragmented rock from large rockslides or rock falls [5], which is usually triggered by factors such as earthquake, rainstorms, glacier melting, and human activities [6, 7]. Iverson [8] proposed that rock avalanche has an extremely complex evolution

mechanism, dominated by erosion, entrainment, and deposition. Some literature has studied this complex process; in the initial sliding stage, the initial internal conditions of the slope, such as the original terrain of the slope, the mechanical properties of rock mass, and the development degree of the structural plane, play a decisive role in the failure mode and fragmentation of the slope [9]; in the process of rock mass movement, the scale is expanded by eroding and wrapping the clastic material of the basement layer, and this process is controlled by many factors such as the amount, density, strength, and saturation of the available basement material on the path [10]; among them, mechanisms such as rapid undrained load effect or ploughing effect can enhance the fluidity of rock mass sliding [11–13], which can increase the disaster scale by 25% to several orders of magnitude [14]. It can be seen that the structural strength and depth characteristics of the base material can affect or limit erosion during debris transportation; however, there is a nonlinear relationship between erosion depth and the change of sliding rock mass volume [14–16], which can be proved by many studies of rock avalanche or debris avalanche (e.g., Erismann.2001; Jibson,2002; Pollet et.al,2004; Bernard et.al, 2009; Huang et.al, 2012; Weidinger et.al,2014; Dufresne et.al, 2015,2016) [17–23].

Although the concept of rock avalanche has been put forward for more than a century, the evolution of such natural disasters is still gaining much attraction these days. The study of a large-scale rock slide or debris avalanche needs to comprehensively analyze the factors such as slope structure and water content, initial failure scale, path topography, and base material structure. As Schilirò et al. [24] pointed out, detailed geological investigation and research are direct and effective in revealing the erosion process during the rock movement. Based on a detailed investigation of LRA, this paper analyzes the clastic sedimentary characteristics of rock avalanches and expounds on the dynamic mechanism of long-distance movement of LRA. The findings can provide a relevant reference for the prediction of similar natural slope disasters and mining slope disasters.

2. Background

The study area is located in the middle of the boundary zone between Sichuan Province and Yunnan Province on the eastern edge of the Qinghai Tibet Plateau, whose geographical coordinates are 102° 18′ 47″ E and 26° 14′ 01″ N (Figure 1). The geological structure is located in the south section of the Sichuan Yunnan structural belt and the west side of the Xiaojiang Fault Zone. In the area, the east-west structural belt, north-south structural belt and northwest structural belt cut each other to form a rhombic fault system. The slope of the study area is located east of the Jinjiaping fault, which roughly extends in the NS direction (Figure 2(a)). The formation lithology consists of grayish black carbonaceous sericite phyllite and grayish black thin-layer slate of Lower Proterozoic Tong'an formation (P_tt). The dip angle of the rock stratum is 18°. The terrain on the west side of the fault is a steep massive mountain landform. The upper part of the mountain is composed of thick dolomite, thin-layer metamorphic quartz sandstone and calcareous schist of Dengying Formation (Z_bd) of Upper Sinian system, and the lower part of the mountain is composed of purplish red feldspathic quartz sandstone and calcareous sandstone of Chengjiang formation (Z_ac) of Sinian system. There are obvious differences in geomorphic characteristics between the upstream and downstream of the Baini cave gully. The landform upstream is a high and steep annular mountain, and an accumulation platform is developed at the foot of the mountain (Figure 2(b)). The bedrock base of the platform is purplish red quartz sandstone of Tongan formation (Pt_1t) with a low dip angle. From bottom to top, the base rock is covered by purplish red sandstone clastic eluvium, a weathered loess layer with a thickness of several meters to tens of meters, and a layer of landslide accumulation. In the middle of the gully, the terrain on both sides is open and presents asymmetry. Quaternary strata are mainly distributed on the right bank, which is gentle and open. It is worth noting that the purple red quartz sandstone rock debris and weathered loess in the ditch bottom area are mainly distributed at the bottom of the avalanche debris layer. Its significance as a marker layer will be discussed in the subsequent chapters.

3. Analytical Methods

In terms of the coverage of LRA, we carried out a detailed geological survey from the source area to the accumulation area and drew and sampled the particle size, composition, and accumulation morphological characteristics of landslide debris in each area in detail. Also, we used high-resolution Google remote sensing images to map the macrolandform of LRA and its surrounding area. Meanwhile, as the basis of a detailed geological survey, Dajiang UAV (Spirit Series) was used to shoot images of a 9.3 km^2 area with a resolution of 0.5 m, with which a digital elevation model (DEM) was created. The macrotopographic index was established by using ArcGIS software, and the statistical method was used to extract the characteristic information from the source area to the accumulation area, such as slope direction, slope, topographic relief, and coarse debris particle distribution. The above detailed geological survey and spatial analysis helped to clarify the fluidization movement sedimentary evolution process of LRA.

4. Result

4.1. The Overall Characteristics. LRA is a large-scale rock slide started from a slope slide at the source of the gully after heavy rainfall. In the process of long-distance transportation, rock mass sliding developed into a large-scale debris avalanche. The overall direction of the movement is N170 ° E, the whole path has a length of 7.3 km, and the maximum drop is 1477 m, leading to an overall slope of 275‰. The horizontal distance from the source area to the distal area is 5.3 km, and the avalanche sediment coverage area is 3.15 km^2. After the disaster, the mainstream of Jinsha River was forced to shift towards Yunnan Province. After the dam burst, the residual debris accumulation slope at the gully mouth reached 60 m high, and the residual slope on the opposite bank was about 30 m. According to the

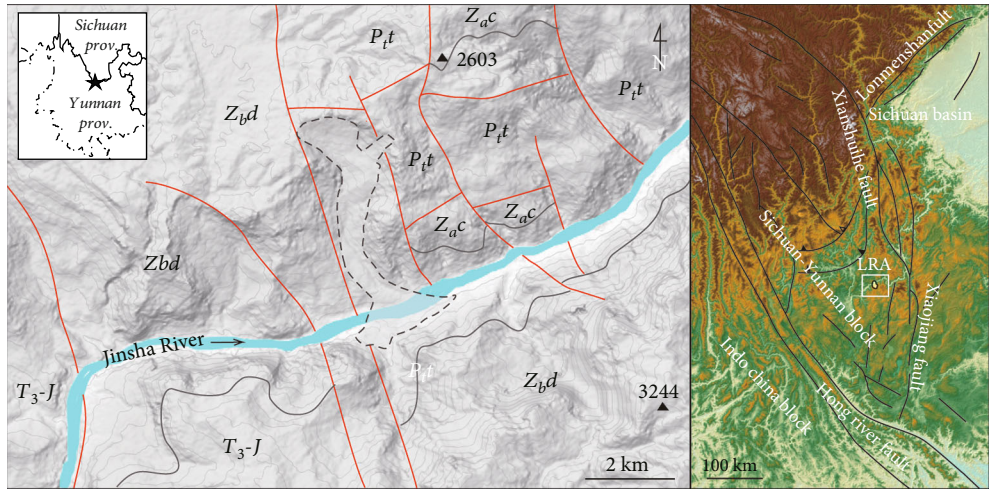

Figure 1: Geographical location and geological background of LRA.

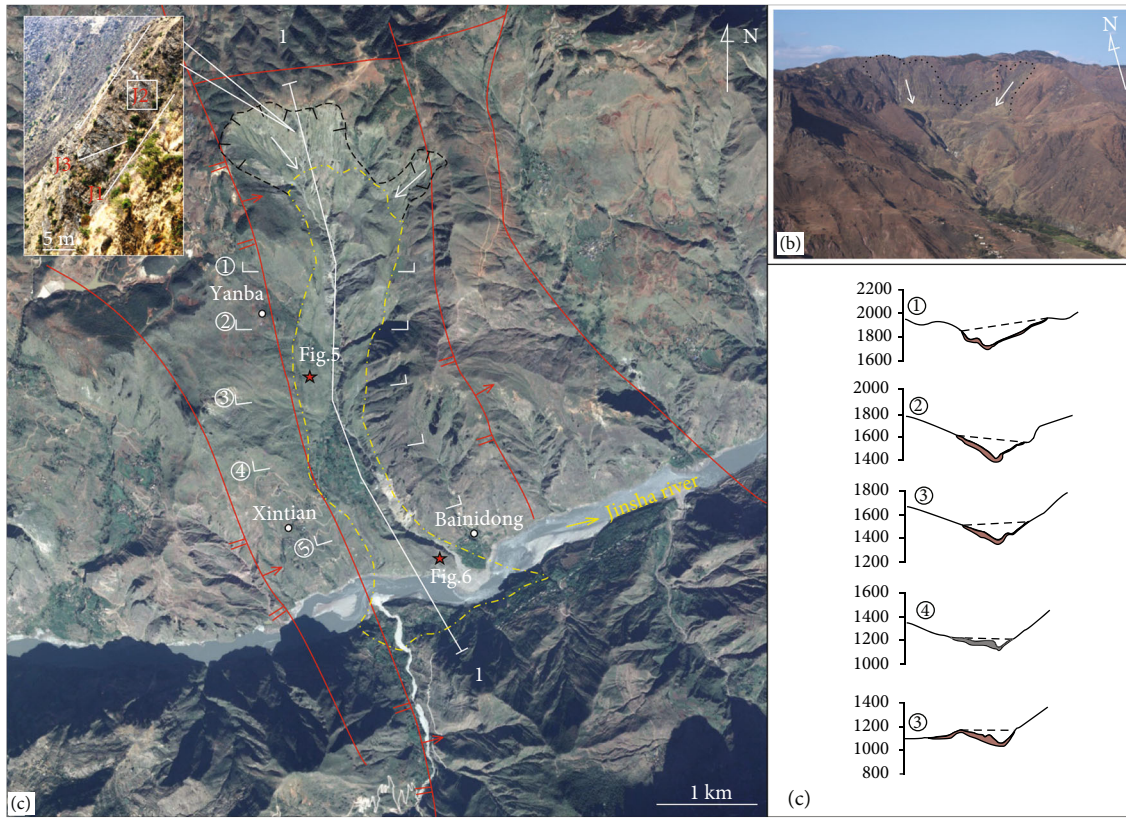

Figure 2: Remote sensing image of LRA and the cross section along the ditch (Google satellite image, 2014)..

conclusion of the detailed geological survey, we divide LRA coverage into three areas: (I) source area, (II) proximal impact area, and (III) distal sedimentary area, as shown in Figure 3. With the gradual decrease of the longitudinal slope of the gully, the gully shape becomes more open, and the mass and thickness of debris tend to be larger. Figure 2(c) shows the transverse sections of the gullies at different elevations.

4.2. Destruction Characteristics of the Source Area. The landform of the LRA source area is a ring-shaped mountain that inclines to the south as a whole. The slope on the west side of the valley forms a tall rock wall along the fault plane. The mountain from the middle to the east of the valley is composed of thin-layer metamorphic rock. Affected by the structure, the attitude of the rock stratum constantly changes, with the altitude varying between 335°and 350°, and ∠

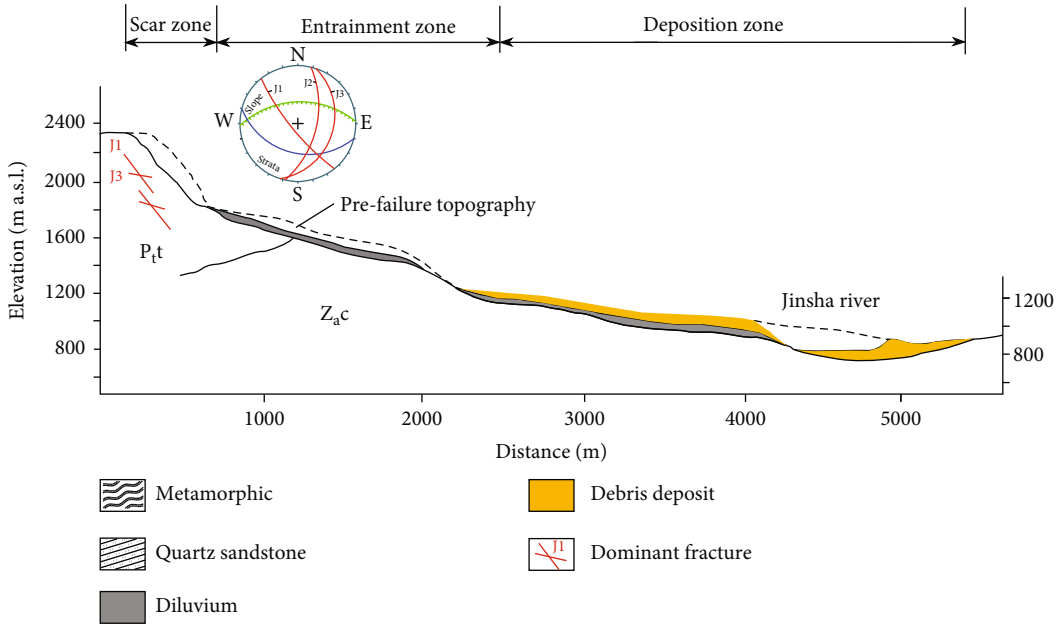

Figure 3: The longitudinal section of LRA.

between 15° and 25°. At a distance from the fault layer, the rock mass structure of the slope gradually changes from plate crack to plate or layered structure.

On the slope rock mass, the main joints have the formations of: ① dip 283°, dip angle 54°; ② dip 51°, dip angle 76°, and the short joints have the formations of ③ dip 288°, angle 27° (see Figure 2(a)). Under the condition of heavy rainfall, the excess pore water pressure formed after rapid infiltration in the fracture zone had caused damage to the deep layer of the slope, which subsequently destroyed the potential wedge of the slope between 2350 m and 1850 m. To estimate the failure volume of LRC, it is necessary to restore the original terrain before slope failure. However, after the disaster in 1935, the slope experienced continuous deformation and expansion, which caused obvious trouble in identifying the initial failure boundary. By combining DEM data analysis with field ground detailed investigation, as well as identifying discontinuous interface and its combination relationship, we found that there are three groups of long joints in Jinjiaping fault and its east area, including two mutually inclined lateral dominant joints, which, respectively, extend in the southeast and west direction, and the slope joint ①, which controls the inner boundary.

According to the distribution range of the damaged wedge, we divided the destructed area of the source area into W1 area and E1 area. The W1 has an irregular shape, and its maximum width is 1.48 km. The height difference from the tensile crack at the trailing edge to the shear outlet at the slope toe is about 370 m, as shown in Figure 4. The damage thickness in this area ranges from 5 m to 50 m. Taking 30 m as the average thickness gives the estimated damage scale of the area as 21.9×10^6 m^3. The E1 is a shallow failure located in the east. A small accumulation fan was developed at the bottom of this area, with a width of 0.3 km and a height of 350 m. Taking 15 m as the average thickness gives the estimated failure scale of E1 as 2.5×10^6 m^3. Therefore, the total failure scale of the slope in the source area is determined as 24.4×10^6 m^3.

The size of debris after failure is controlled by rock joints and metamorphic rocks on the surface and usually cannot exceed 2 m. After the failure, four hummocks were formed in the slope zone (Figure 4(a)), and their positions were staggered, indicating that they came from different source areas and accumulation processes.

4.3. The Proximal Impacted Area. The proximal impacted area refers to the area from the slope toe of the source area to the middle reaches of the valley, with a distribution elevation of 1850 m to 1230 m and a plane length of 1.9 km. It is mainly composed of two deep gullies, and the trend of the valley gradually deflects in an arc from the steep slope section. The bank slopes on two sides form an open asymmetric valley with an overall gradient of 285‰. There is a deep residual deluvial soil layer at the bottom of the original gully. Rainfall before the landslide increased the water content of liquefiable soil. After being impacted by the rock avalanche, liquefaction undoubtedly occurred here. The flow state of the debris avalanche is affected by the valley terrain, which can produce scraping, dispersion, sprinkling, and other forms. Between the platform area at the foot of the slope in the source area and the steep slope section below, the avalanche fluid entrained a large number of eluvial diluvium. Thus, this is the main area where the avalanche volume expanded.

With the undulation of valley terrain, the main body of the debris avalanche has significant lateral expansion and dispersion in the process of advancing. At the same time, the direction of the valley is deflected by 170°. The avalanche has obvious curve superelevation at the deflection, with a maximum height of more than 60 m, and forms a raised

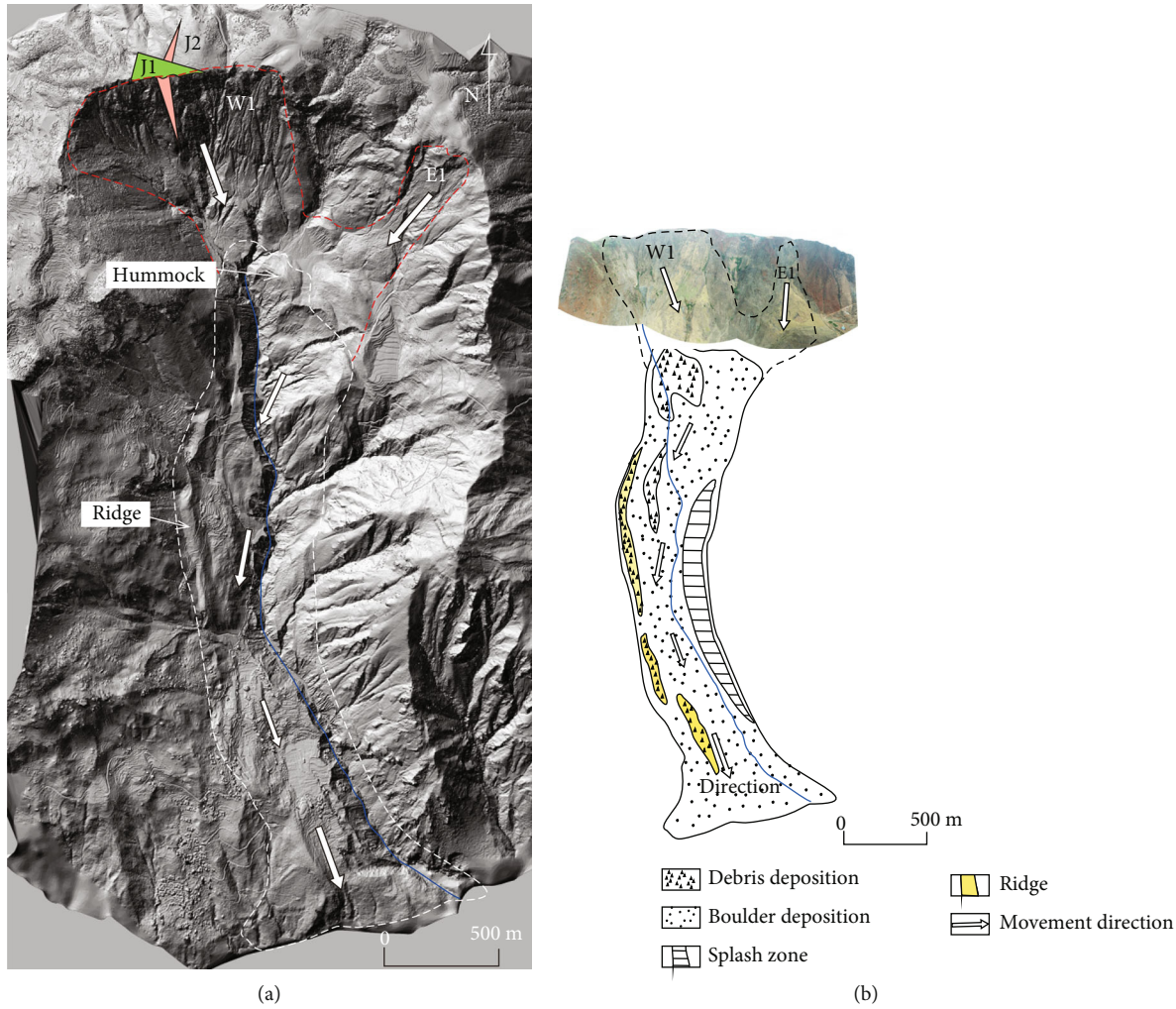

Figure 4: (a) Structural analysis of DEM mountain image in the source area and (b) the zoning map of sedimentary evolution.

longitudinal ridge at the edge of the right bank (Figure 4(a)). The raised height of the longitudinal ridge body ranges from 10 to approximately 30 m and extends to the ditch mouth. The profile outside the ridge reveals that its internal structure is a transition from the loose structure with coarse breccia on the surface to the breccia soil layer inside (Figure 5). Since the right bank slope is composed of thick dolomite, we speculate that the liquefied soil layer at the bottom of it comes from the upstream entrainment, which enhances the fluid fluidity and lateral expansion ability.

The debris accumulation structure on the left bank is obviously different from that on the right bank. At present, the volume of debris remaining on the surface of the slope on the left bank is much lower than that on the right bank. Its main component is fine debris accumulated on the side edge of the ditch, forming an intermittent flow platform (Figure 6). Because phyllite fine-grained debris is the suitable soil for the growth of gramineous plants, the distribution range of specific gramineous plants can be clearly identified in the high-precision satellite impact map (see Figure 2), which makes it an important reference for distinguishing the lateral boundary of the debris avalanche deposits. However, the survey shows no obvious trace of impact and erosion on the left bank slope. At present, the residual clastic accumulation structure here is mainly fine breccia. Therefore, we speculate that the accumulation area of the edge slope is the "splash area" of dry debris (Figure 6). Still, we do not rule out that it may be the residual structure after the fluid front with the main property of solid-gas two-phase mixture passes through the slope. This feature is rarely developed on the right bank. Although it is difficult to accurately calculate the content of entrained debris in the entrainment area, it is certain that the rock avalanche has produced an entrainment process in the residual soil layer at the bottom of the ditch in this area, which significantly expands the scale of the avalanche and constitutes an important condition for the growth distance movement of Luchedu rock avalanche.

4.4. Distal Sedimentary Area

4.4.1. The Avalanche Scale. The distal sedimentary area of LRA is distributed from the destroyed upper yanba village to the opposite bank of Jinsha River in the downstream direction, with an altitude ranging from 1230 m to 880 m. The longitudinal profile of this area is a multilevel gentle

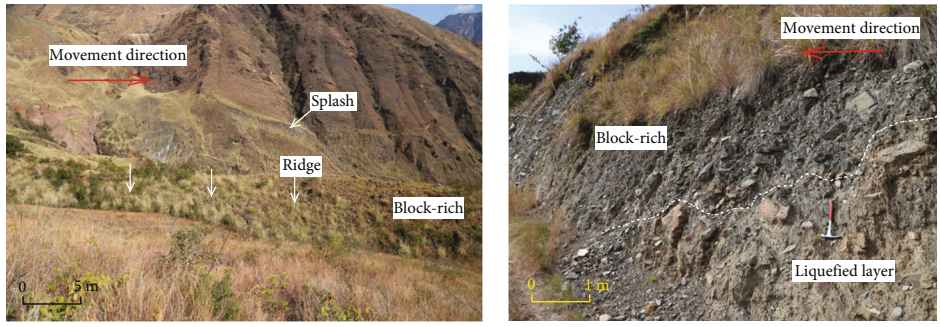

(a) (b)

Figure 5: The sedimentary structure in the edge direction of the proximal area of the Luchedu rock avalanche (see Figure 2 for the corresponding position). (a) A raised longitudinal ridge at the edge of the right bank, debris accumulation at the bottom of the ditch on the left bank, and splash area on the slope. (b) The internal sedimentary structure on the inner side of the road (a liquefied loess layer with metamorphic rock breccia lies at the bottom).

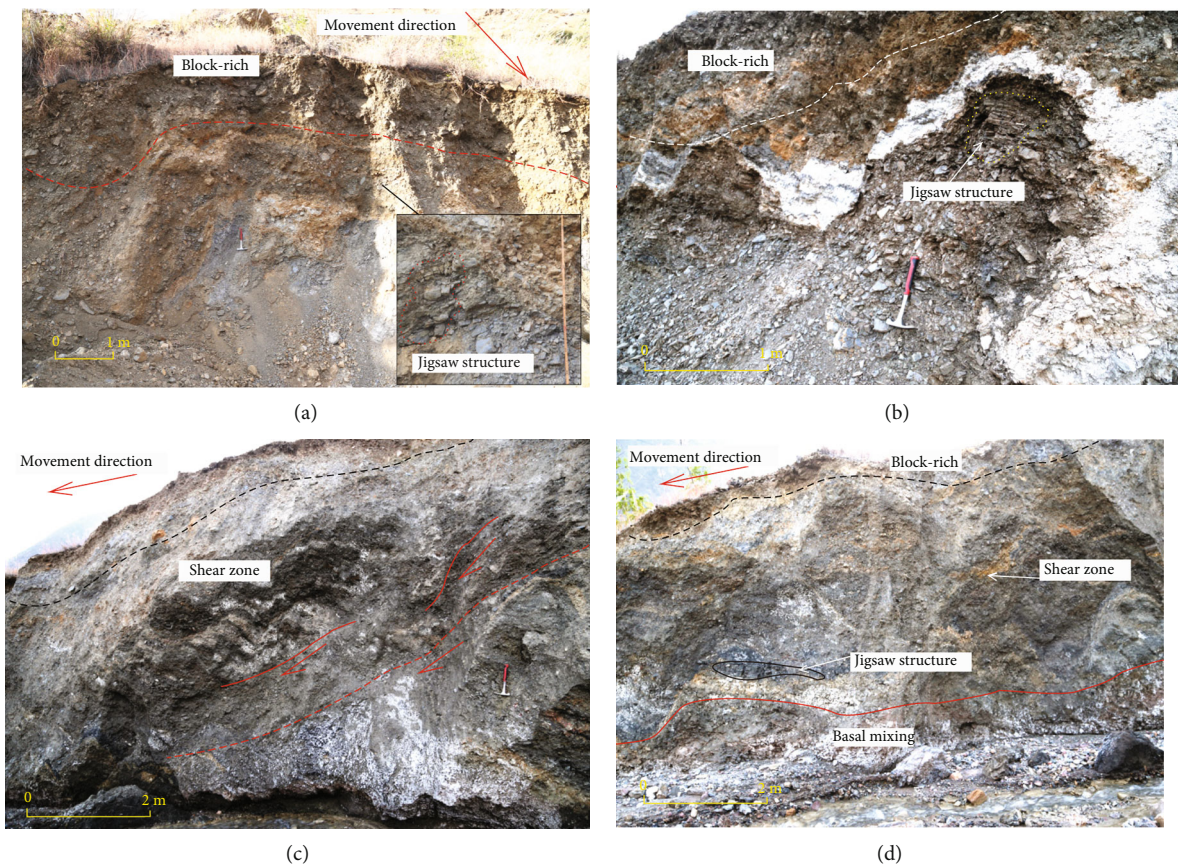

(a) (b)

(c) (d)

Figure 6: Internal structural features of sediments taken from distal deposits of Luchedu rockfall. (a) The puzzle structure of broken and sheared materials on the surface about 4.8 km away from the source. (b) Liquefied soil interlayer. (c) Multishear band deformation. (d) Purplish red clastic mixed zone at the bottom.

descending platform with a stacking length of 2.7 km. The sedimentary thickness gradually increases in the downstream direction, and the maximum thickness is located in the Jinsha River valley belt (see Figure 3). The mouth of the original channel was blocked by rock avalanche accumulation, and lots of debris rushed out from the bank slope on the left side of the mouth, resulting in the blockage of Jinsha River.

In order to estimate the total amount of accumulation as accurately as possible, we drew the typical profile of each section according to the high-precision DEM obtained from the UAV image and calculated the volume of each section. Vertically, the thickness of debris accumulation is between 5 m and 80 m, the maximum thickness area is at the bottom of the valley, and the accumulation thickness is between 50 m and approximately 65 m. The estimated volume of

distal accumulation is $50.5 \times 10^6\ m^3$. Considering that the well-exposed accumulation profile is mainly in the longitudinal direction and there is no good exposure in the transverse direction, this estimation may not be accurate.

4.4.2. Sedimentary Structure and Facies. The clasts in the distal sedimentary area of LRA are mainly slate and phyllite clasts, as well as purplish red feldspathic quartz sandstone and weathered loess entrained from the upstream valley. Among them, weathered loess is mainly distributed in the lower part of the accumulation layer and mixed with metamorphic rock debris. The basement layer is composed of all kinds of loose breccia soil and contains a small part of rock slide debris. The grain size composition of clastic particles covers the range from giant breccia to clay particles. In particular, the particle size of giant breccia is mostly within 2 m and distributed in the surface area of the outer edge ridge of the proximal area and the distal area. The sedimentary structure of LRA has significant stratification characteristics, and the clastic layers with different particle sizes and stacking structures constitute different sedimentary units. The typical sedimentary structure is divided into three layers, and the main sedimentary facies types correspond to carapace facies, body facies, and basement mixed facies.

(1) Carapace facies is a common surface sedimentary structure of rock avalanches of similar scale (literature). The upper crust phase of LRA is a particle size matrix structure containing giant breccia, in which the content of coarse breccia with the particle size of 10~30 cm is the highest (Figure 6(a)). In the profile, we can see the liquefaction strips with thickness ranging from 3 to 10 cm and abundant jigsaw structures, which are mainly composed of metamorphic rock blocks with the diameter ranging from 10 cm to 1 m. The primary schistosity structure is retained inside, which is basically in a gently inclined attitude and can be covered or wrapped by liquefied soil layer, revealing the laminar flow property of surface structure and limited internal deformation characteristics

(2) The body facies, which account for the main part of the LRA sedimentary structure, is composed of fine breccia clasts containing coarse breccia and is mainly characterized by the development of densely arranged and nearly horizontal shear zones. The development thickness of a single shear zone is usually between 2 m and 10 m, with an interval of tens of centimeters to several meters, showing white and dark flat bands in appearance (Figure 6(b)). After equivalent grinding effects, the internal particles have become fine particles, powder particles, and even clay particles. The flake rock fragments in the body facies are nearly parallelly arranged. The change of clastic particle size is significant vertically and has good continuity horizontally, thus forming a structural form similar to bedding (Figure 6(c)). Under the action of overlying pressure, the shear zone and flake clastic particles often deform or deflect in the same direction, resulting in local fault structures. There are still jigsaw structures in the body facies, but the development degree and block ratio are not as obvious as the surface layer

(3) The lower part is a mixed facies, which is mainly composed of soil fine breccia layer. The breccia composition includes rock debris and sediments from the gully bottom residual and the source area, including purplish red sandstone containing clastic soil layer and weathered loess layer (Figure 6(d)). The silt content is between 10% and approximately 20%. Shear zones and local jigsaw structures are developed in this layer, and the particle size of clastic material here is further reduced. The mixed facies is formed by avalanche entrainment. After moving to the distal area, the avalanche debris is gradually compacted and thinned and mixed with the liquefied soil layer to produce near-horizontal shear movement, which leads to the uniform arrangement of flake debris particles. Such a structural form can reduce the friction coefficient at the bottom of the fluid and plays a significant role in long-distance transportation

4.4.3. Particle Analysis Experiment. The distal area of LRA shows a good sedimentary profile, and the macrosedimentary characteristics show that the size of clastic particles gradually increases from bottom to top. Samples taken from the profile close to the river bank were used to conduct the indoor particle analysis experiment (see Figure 6(a)). In order to make the sample representative, samples from the upper, middle, and lower layers of the profile were all used to determine the particle grading number (Figure 7). According to the experimental analysis, the sorting coefficient is less than 1.27. Therefore, in the distal region, the reverse distribution of particles is the main feature of the sedimentary structure. The causes of the feature include the vibration screening of surface particles and the shear crushing of underlying clastic particles.

5. Discussion

5.1. The Entrainment Rate of LRA. The above contents estimate the slope failure scale in the source is and accumulation scale in the distal area of LRA. As discussed elsewhere [8, 25], erosion, entrainment, and deposition are the dominant mechanical processes in rock avalanche, but the erosion and entrainment mechanism of rock avalanches has not been fully explained for a long time and the scale of volume development is often underestimated. Referring to the study on the contribution of entrainment to the scale expansion of rock avalanche [26], the entrainment rate is defined as the ratio between the volume of debris captured from the path and the expansion volume of rock debris generated by initial rock failure, and the calculation formula is

$$ER = \frac{V_{\text{entrained}}}{V_{\text{fragmented}}} = \frac{V_E}{V_R(1 + F_F)}. \quad (1)$$

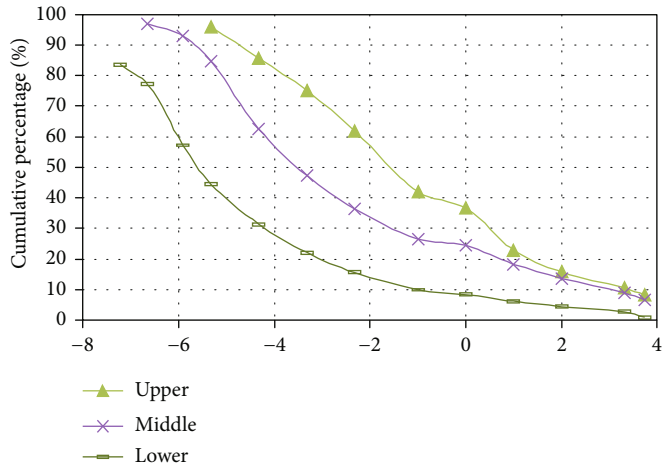

Figure 7: Sediment particle analysis in the distal area of LRA.

According to this formula, the entrainment rate of LRA is 1.2. Generally, the entrainment rate decreases with the increase of the scale of the rock avalanche. The entrainment rate of a large-scale rock avalanche (>106 m^3) is mainly distributed between 0.25 and 1.5. Noe should notice that the entrainment rate of LRA is high compared to rock avalanches at other scales. Therefore, the entrainment rate of LRA is obviously not determined by the scale effect. Lithology and other factors are likely to play a more key role.

5.2. Laminar Flow in the Distal Area of LRA. The sedimentary facies of LRA mainly include carapace facies, body facies, and mixed facies. There are irregular giant breccia patches on the plane of avalanche sedimentary area, and scattered and discontinuous jigsaw structures are developed inside. Many studies have shown that mosaic structure in the body facies represents the finite internal deformation in the process of rock avalanche propagation, and the sharp contact structure at the boundary indicates the transportation process only received limited disturbance (e.g., [23, 27–29]). In addition, it is considered that the inverse grading of particles is a typical feature of the sedimentary structure of the rock avalanche [10, 30–32]. In the investigation of LRA, it is found that the structures with reversely distributed particles can be observed in the stacking profiles in the proximal and distal regions, and the reverse particle size in the proximal region is mainly related to dynamic screening and fragmentation–spreading model. According to the typical sedimentary characteristics of LRA, it can be speculated that its distal evolution has characteristics of laminar flow.

5.3. Long-Distance Movement under the Control of Entrainment and Lithology. Many studies on rock avalanches have focused on the mechanism of long-distance transportation, Theoretical hypotheses on the cause include the theory of inviscid particle flow, the theory of air cushion, and the theory of trapped air causing fluidization wave [10, 27, 31, 33–37]. However, all the above theories have limitations in applicability [9].

In open terrain, the transportation form of rock avalanche is affected by friction shear. Generally, the farther the propagation distance is, the more obvious the lateral diffusion is [13]. The transportation process is controlled by the ploughing effect and entrainment. In contrast, rock avalanches in typical valley terrain are additionally affected by the lateral collision and undulating ground. The structural deformation and horizontal shear in the sedimentary area of the distal area of LRA are significant, which is mainly determined by the material. The above investigation shows that the abnormally developed shear layer in the LRA sediment and the regular sorting and arrangement of clastic particles greatly enhanced the fluidity of rock avalanche quality in the distal area. The reason is that the slate and phyllite are prone to fragmentation and directional arrangement in the process of vibration and compaction. In addition, considering the shear zone is not thick enough, the internal debris particles become smaller due to grinding, which further reduces the friction coefficient of shear resistance. Consequently, the horizontal shear stress is limited to a smaller range under the action of laminar flow, which greatly reduces the internal energy loss in the transportation process.

From above, the long-distance transportation of LRA is not only related to the high entrainment rate but also closely related to the accumulation structure composed of slate and phyllite clastic particles. These two factors played an important role in the avalanche movement throughout the stages. After the occurrence of the rock slide, the rock debris began to slide rapidly, and the entrainment in the proximal region made the scale of the slide expand rapidly. At the same time, the base liquefaction layer ensures the rapid movement of fluid. When the avalanche reached the distal region, the thickness of the bottom mixing layer expanded, and the development of directionally arranged flake debris particles and shear zone reduced the energy loss of fluid movement. Such laminar flow obviously promotes the fluid transport above the mixing zone, which is of great significance for the inlet section of the gully, where the base topography changes significantly. Therefore, the long-distance

transportation of LRA is controlled by specific lithology, which is obviously different from other types of rock avalanches such as limestone or granite.

6. Conclusions

The Luchedu rock avalanche (LRA) in 1935 is described in detail in this paper. This catastrophic landslide was formed inside the rhombic fault system, where regional structures were active. A huge wedge-shaped body composed of quartz slate and phyllite slate was separated along a fault with dolomite as the boundary. The rock fragments were transported along a 7.3 km arc undulating path, with a horizontal span of 5.3 km and a vertical drop of 1477 m, resulting in the blockage of Jinsha River. Due to the steep curved path and the significant lateral movement of high-speed fluid during entrainment, this avalanche showed strong fluidity and created a curve superelevation up to 55 m.

LRA was triggered by heavy rainfall, and a large amount of debris formed after rock avalanche damage was washed down from the source area, with an entrainment rate of 1.2, making it an interesting case for studying large rock avalanches under complex gully terrain. In this paper, we have gained the following understanding through a detailed geological survey:

(1) Many intact avalanche sedimentary structures are preserved in the field. Through the detailed analysis of these sedimentary structures, we discussed the process of LRA destruction, transportation, and accumulation. In the source area, under the influence of heavy rainfall, the slope was subjected to excess pore water pressure after being saturated, resulting in sliding separation of the unstable wedge along the deep boundary

(2) The entrainment process mainly occurred in the steep valley drop zone near the avalanche. In the process, the purplish red quartz sandstone and weathered loess layer on the original surface were scraped and shoveled. The entrainment gradually thinned in the process of migration and mixed with metamorphic rock debris in the distal area

(3) The sedimentary structure of LRA is basically composed of three types of lithofacies: carapace facies, body facies, and mixed facies. There are near horizontal shear zones and jigsaw structures in the bulk and mixed phases, indicating that only limited deformation has occurred in the fluid, so the movement in the distal region is mainly in the form of laminar flow

(4) Compared with other lithologic types, the development of the primary schistosity of slate and phyllite is the basic condition for the specific accumulation structure of LRA. It is also one of the primary conditions for continuous development of the fluid movement in the distal region

In the deep valley area of Jinsha River in southern Sichuan, similar potential threats of high-mobility rock avalanches may also exist, which will cause adverse effects and potential heavy losses to the reservoir area of Wudongde Hydropower Station, China's third largest hydropower station. Since similar geological and topographical conditions are quite common, more research attention should be paid to this topic.

Data Availability

All the data were obtained from the author's test.

Conflicts of Interest

The authors declare that they have no conflicts of interest.

Acknowledgments

This research was funded by the National Key Research and Development Project of China (2018YF C1505000). Thank you very much to Professor Deng Jianhui of Sichuan University, Professor Wen Baoping of China University of Geosciences (Beijing) and Professor Dai Fuchu of Beijing University of Technology for their guidance.

References

[1] Y. F. Shi, B. X. Tang, and B. Xu, *Investigation of a giant landslide in Pufugou (Lannigou)*, Luquan, Yunnan, 1993.

[2] R. Huang, X. Pei, X. Fan, W. Zhang, S. Li, and B. Li, "The characteristics and failure mechanism of the largest landslide triggered by the Wenchuan earthquake, May 12, 2008, China," *Landslides*, vol. 9, no. 1, pp. 131–142, 2012.

[3] J. W. Zhou, P. Cui, and M. H. Hao, "Comprehensive analyses of the initiation and entrainment processes of the 2000 Yigong catastrophic landslide in Tibet, China," *Landslides*, vol. 13, no. 1, pp. 39–54, 2016.

[4] Q. Chen, G. Fan, and J. W. Zhou, "Numerical simulation of the 2017 xinmo catastrophic landslide considering entrainment effect," *Frontiers in Earth Science*, vol. 8, article 537800, 2020.

[5] O. Hungr, S. G. Evans, M. M. Bovis, and J. N. Hutchinson, "A review of the classification of landslides of the flow type," *Environmental & Engineering Geoscience*, vol. 7, no. 3, pp. 221–238, 2001.

[6] S. G. Evans, J. J. Clague, G. J. Woodsworth, and O. Hungr, "The pandemonium creek rock avalanche, British Columbia," *Canadian Geotechnical Journal*, vol. 26, no. 2, pp. 427–446, 1989.

[7] S. G. Evans, O. Hungr, and J. J. Clague, "Dynamics of the 1984 rock avalanche and associated distal debris flow on Mount Cayley, British Columbia, Canada; implications for landslide hazard assessment on dissected volcanoes," *Engineering Geology*, vol. 61, no. 1, pp. 29–51, 2001.

[8] R. M. Iverson, "Elementary theory of bed-sediment entrainment by debris flows and avalanches," *Journal of Geophysical Research: Earth Surface*, vol. 117, no. F3, article F03006, 2012.

[9] T. R. Davies, M. J. McSaveney, and K. A. Hodgson, "A fragmentation-spreading model for long-runout rock avalanches," *Canadian Geotechnical Journal*, vol. 36, no. 6, pp. 1096–1110, 1999.

[10] K. Sassa, "Geotechnical model for the motion of landslides (special lecture)," *Proc. 5th Inter. Symp. On Landslide*, vol. 1, pp. 37–56, 1989.

[11] K. Sassa, "The mechanism of debris flows," *In Proceedings of the 11th International Conference on Soil Mechanics and Foun dation Engineering San Francisco*, vol. 1, pp. 1173–1176, 1985.

[12] A. Yin and M. H. Taylor, "Mechanics of v-shaped conjugate strike-slip faults and the corresponding continuum mode of continental deformation," *Geological Society of America Bulletin*, vol. 123, no. 9-10, pp. 1798–1821, 2011.

[13] Y. F. Wang, Q. G. Cheng, A. W. Shi, Y. Q. Yuan, Y. H. Qiu, and B. M. Yin, "Characteristics and transport mechanism of the Nyixoi Chongco rock avalanche on the tibetan plateau, China," *Geomorphology*, vol. 343, pp. 92–105, 2019.

[14] S. G. Evans, N. F. Bishop, L. F. Smoll, P. V. Murillo, K. B. Delaney, and A. Oliver-Smith, "A re-examination of the mechanism and human impact of catastrophic mass flows originating on Nevado Huascaran, Cordillera Blanca, Peru in 1962 and 1970," *Engineering Geology*, vol. 108, no. 1-2, pp. 96–118, 2009.

[15] L. Le and E. B. Pitman, "A model for granular flows over an erodible surface," *SIAM Journal on Applied Mathematics*, vol. 70, pp. 1407–1427, 2009.

[16] W. Liu, D. Wang, J. Zhou, and S. He, "Simulating the Xinmo landslide runout considering entrainment effect," *Environment and Earth Science*, vol. 78, no. 19, p. 585, 2019.

[17] T. H. Erismann and G. Abele, *Dynamics of Rockslides and Rockfalls*, Springer Science & Business Media, Berlin,Germany, 2001.

[18] R. W. Jibson, E. L. Harp, W. Schulz, and D. K. Keefer, "Large rock avalanches triggered by the M 7.9 Denali Fault, Alaska, earthquake of 3 November 2002," *Engineering Geology*, vol. 83, no. 1-3, pp. 144–160, 2006.

[19] N. Pollet and J. Schneider, "Dynamic disintegration processes accompanying transport of the Holocene Flims sturzstrom (Swiss Alps)," *Earth & Planetary Science Letters*, vol. 221, no. 1-4, pp. 433–448, 2004.

[20] B. Bernard, B. V. W. de Vries, D. Barba et al., "The Chimborazo sector collapse and debris avalanche: deposit characteristics as evidence of emplacement mechanisms," *Journal of Volcanology & Geothermal Research*, vol. 176, no. 1, pp. 36–43, 2008.

[21] J. T. Weidinger, O. Korup, H. Munack et al., "Giant rockslides from the inside," *Earth & Planetary Science Letters*, vol. 389, pp. 62–73, 2014.

[22] A. Dufresne, C. Prager, and J. J. Clague, *Complex Interactions of Rock Avalanche Emplacement with Fluvial Sediments: Field Structures at the Tschirgant Deposit*, Springer International Publishing, Austria, 2015.

[23] A. Dufresne, A. Bsmeier, and C. Prager, "Sedimentology of rock avalanche deposits - case study and review," *Earth-Science Reviews*, vol. 163, pp. 234–259, 2016.

[24] L. Schilirò, C. Esposito, F. V. De Blasio, and G. Scarascia Mugnozza, "Sediment texture in rock avalanche deposits: insights from field and experimental observations," *Landslides*, vol. 16, no. 1160, pp. 1629–1643, 2019.

[25] C. Huggel, S. Zgraggen-Oswald, W. Haeberli et al., "The 2005 rock/ice avalanche at Kolka/Karmadon, Russian Caucasus: assessment of extraordinary avalanche formation and mobility, and application of QuickBird satellite imagery," *Natural Hazards & Earth System ences*, vol. 5, no. 2, pp. 173–187, 2005.

[26] O. Hungr and S. G. Evans, "Entrainment of debris in rock avalanches: an analysis of a long run-out mechanism," *Geological Society of America Bulletin*, vol. 116, no. 9, pp. 1240–1252, 2004.

[27] R. Shreve, "Sherman landslide, alaska," *Science*, vol. 154, no. 3757, pp. 1639–1643, 1966.

[28] A. L. Strom and O. Korup, "Extremely large rockslides and rock avalanches in the Tien Shan Mountains, Kyrgyzstan," *Landslides*, vol. 3, no. 2, pp. 125–136, 2006.

[29] Y. F. Wang, Q. G. Cheng, Q. W. Lin, K. Li, and H. F. Yang, "Insights into the kinematics and dynamics of the Luanshibao rock avalanche (Tibetan Plateau, China) based on its complex surface landforms," *Geomorphology*, vol. 317, pp. 170–183, 2018.

[30] D. Hungr, "The debris of the Frank Slide and theories of rockslide–avalanche mobility," *Canadian Journal of Earth Sciences*, vol. 23, no. 3, pp. 425–432, 1986.

[31] S. A. Dunning, "The grain-size distribution of rock avalanche deposits in valley-confined settings," *Italian Journal of Engineering Geology & Environment*, vol. 1, pp. 117–121, 2006.

[32] P. E. Kent, "The transport mechanism in catastrophic rock falls," *Journal of Geology*, vol. 74, no. 1, pp. 79–83, 1966.

[33] K. J. Hsu, "Catastrophic debris streams (Sturzstroms) generated by rockfalls," *Geol Soc America Bull*, vol. 86, no. 1, pp. 129–129, 1975.

[34] T. H. Erismann, "Mechanisms of large landslides," *Rock Mechanics*, vol. 12, no. 1, pp. 15–46, 1979.

[35] T. Davies, "Spreading of rock avalanche debris by mechanical fluidization," *International Journal of Rock Mechanics & Mining Sciences & Geomechanics Abstracts*, vol. 15, no. 1, pp. 9–24, 1982.

[36] P. Tapponnier, F. J. Ryerson, J. Van der Woerd, A. S. Mériaux, and C. Lasserre, "Vitesses de glissement a long terme et dislocations cosismiques caracteristiques : cles du fonctionnement des failles actives et de l'alea sismique," *Comptes Rendus de l'Academie des Sciences Series IIA Earth and Planetary Science*, vol. 333, no. 9, pp. 483–494, 2001.

[37] J. Orwin, J. Clague, and R. Gerath, "The Cheam rock avalanche, Fraser Valley, British Columbia, Canada," *Landslides*, vol. 1, no. 4, pp. 289–298, 2004.